

Dynamic mechanisms for shear-dependent apparent slip on hydrophobic surfaces

Eric Lauga & Michael P. Brenner

Division of Engineering and Applied Sciences, Harvard University,
29 Oxford Street, Cambridge, MA 02138.

(dated: December 22, 2018)

Recent experiments (Zhu & Granick (2001) Phys. Rev. Lett. 87 096105) have measured a large shear dependent fluid slip at partially wetting fluid-solid surfaces. We present a mechanical model for such slip, motivated by the recent observations of stable nanobubbles on hydrophobic surfaces. The model considers the dynamic response of nanobubbles to change in hydrodynamic pressure. Both the compression and diffusion of gas in the bubbles decrease the viscous force by a "leaking mass" effect, thereby creating an apparent shear-dependent slip. With nanobubbles similar to those observed by atomic force microscopy to date, the model is found to reproduce the major features of the experimental measurements, independently of the details of the mechanism stabilizing the nanobubbles against dissolution.

I. INTRODUCTION

The validity of the no-slip boundary condition is at the center of our current understanding of fluid mechanics. It remains however an assumption whose microscopic validity has been widely debated [1]. The widespread acceptance of the no-slip condition is based on a historical record of outstanding agreement between theories and experiments. It is commonly agreed [2, 3, 4] that the no-slip condition results from inevitable microscopic roughness, which causes enough viscous dissipation to effectively bring the fluid to rest near the surface. Remarkably, this explanation is independent of the nature of the solid and the liquid, contrary to ideas first proposed by Girard (see [1]).

The development of small devices has recently prompted a reexamination of fluid slip on length scales of nanometers and microns, both experimentally [2, 5, 6, 7, 8, 9, 10, 11, 12] and theoretically [13, 14, 15, 16, 17, 18, 19]. The degree of slip is usually quantified by a slip length

$$l_s = \frac{U_s}{\dot{\gamma}}; \quad (1)$$

where U_s is the slip velocity and $\dot{\gamma}$ is the liquid strain rate evaluated at the surface; equivalently, l_s is the distance below the solid surface where the velocity extrapolates to zero linearly [20]. In experiments, slip is usually found when the liquid partially wets the solid surface; measured slip lengths span four orders of magnitude, from liquid mean free paths to microns, and are usually shear-dependent in squeeze flow experiments, with l_s an increasing function of $\dot{\gamma}$. In particular, Zhu & Granick [8] report squeeze flow experiments, in which two crossed cylinders oscillate about a fixed average distance. By measuring the viscous resistance, Zhu & Granick extracted the slip length over a wide range of oscillation amplitudes. These experiments lead to the largest shear-dependent slip lengths yet (up to $2 \mu\text{m}$).

The origin of this large shear dependent slip is heretofore mysterious. Nanobubbles have recently been observed on hydrophobic surfaces, using atomic force microscopy, with typical thickness $h \approx 10 \text{ nm}$, typical radius $R \approx 50 - 100 \text{ nm}$ and high surface coverage [21, 22, 23, 24]. Although the origin of these bubbles remains unclear, they have been often invoked as a possible origin of the so-called hydrophobic attraction [25, 26, 27, 28, 29] and their existence points to a possible picture for such large slip, as pointed out by de Gennes [19].

It is well known that there is slip at a solid-gas interface, and therefore it is natural to wonder whether the existence of such a gas layer at the solid surface is sufficient to explain the experiments. When a fluid of viscosity η_1 adjoins a layer of fluid of thickness h with smaller viscosity η_2 , the discontinuous strain rate at the fluid-fluid interface results

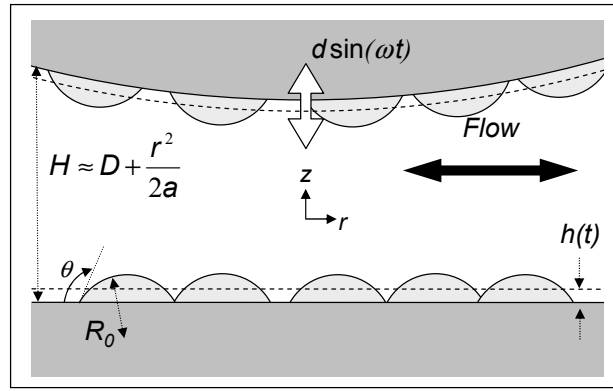


FIG. 1: Typical squeeze flow experiment: a solid sphere of radius a is oscillated in a liquid at a distance D of a smooth solid surface with amplitude $d \sin(\omega t)$ and frequency ω . The surface is covered by microscopic gas bubbles of contact angle θ and radius of curvature R_0 . The set of bubbles is approximated by a gas layer of time evolving thickness $h(t)$.

in an apparent slip with slip length

$$l_s = h \frac{1}{2} \quad (2)$$

Choosing $\lambda_1 = \lambda_2 = 50$ appropriate for a gas-water interface leads to slip lengths as large as 500 nm. This estimate is however independent of the interfacial shear and therefore unable to explain the shear dependence of the slip lengths reported in squeeze flow experiments; it also overestimates the slip length in the case of bubbles, as is discussed in section V. Note however that similar arguments are consistent with data from pressure-driven flow experiments where reported slip lengths are essentially shear-independent [10, 11, 18, 30, 31, 32].

In this article, we will assume stable nanobubbles exist on hydrophobic surfaces and will calculate their dynamic response to an imposed oscillatory shear. In an oscillatory squeeze flow experiment [8], we argue that the pressure fluctuations in the fluid cause the nanobubbles to act as a "leaking mattress", with both compression and dilation of the gas in the bubble, as well as diffusion of gas into (and out of) the bubble. Both of these effects decrease the force required to move the plates, and hence create an apparent slip.

Our calculations, which rely on the existence of stable nanobubbles through an as yet unknown mechanism, indicate that the magnitude of this slip is consistent with the observations of Zhu & Granick as long as the bubble radius is in the range 10–200 nm and the surface coverage is 90%. These numbers are consistent with experimental observations of nanobubbles to date and are found to be independent of the details of the stabilizing mechanism.

II. PHYSICAL PICTURE

A typical oscillatory squeeze flow experiment is shown in Figure 1: a sphere of radius a oscillates with velocity V_s in a viscous liquid of viscosity η at a distance D of a planar surface. The sphere and the surface are assumed to have the same surface characteristics. The lubrication force opposing the motion of the oscillating sphere is given by

$$F_{\text{lub}} = \eta f \frac{6a^2}{D} V_s \quad (3)$$

If the no-slip boundary condition is satisfied then $f = 1$ and any deviation $f < 1$ is interpreted as fluid slip, with a slip length on both surfaces inferred from [33]

$$f = \frac{D}{3} \left(1 + \frac{D}{6} \ln \left(1 + \frac{6}{D} \right) \right)^{-1} \quad (4)$$

If however we assume that the two surfaces are covered with nanobubbles (see Figure 1), the vertical viscous force is given by

$$F(t) = f \frac{6 a^2}{D} V_s \frac{dh}{2 dt} \quad (5)$$

where h is an average bubble thickness on each surface, f is given by (4) with the appropriate slip length for flow over a distribution of bubbles (f is constant if $d \ll D$) and the factor 2 accounts for the fact that each surface is covered with bubbles.

Hence, a time dependent mean bubble size $h(t)$ in equation (5) gives a natural way of modifying the viscous force. Indeed, we will show in what follows that small pressure fluctuations in the fluid gap lead to a first-order linear relation between the rate of change of the mean bubble height and the viscous force, $\dot{h} = (k_1 F + k_2 \dot{F})$, where k_1 and k_2 are positive and shear-dependent; k_1 and k_2 represent respectively the "leaking" and "mass" effects. If the sphere oscillates at frequency ω , equation (5) thereby leads to a new effective force ratio $\bar{f} < 1$, smaller than that obtained by slip on the bubble surface f and given by:

$$\bar{f} = \frac{f}{1 + \frac{12 a^2 k_1 f}{D} + \frac{12 a^2 \omega k_2 f}{D^2} \frac{f}{1 + \frac{12 a^2 k_1 f}{D}}} \quad (6)$$

We present in what follows a model leading to the values of $(k_1; k_2)$, and then compare to the Zhu & Granick experiments and available data on nanobubbles.

III. NANOBUBBLE STABILITY

We need to study the response of nanobubbles to an oscillating pressure in the fluid. We suppose that a number density n of identical gas nanobubbles cover the bottom surface (in Figure 1), undeformed by viscous stresses (this assumption limits the range of ω and a considered by the model), and take h to be the average bubble thickness; we also neglect bubble interactions.

To perform the calculation, it is necessary to have a model for nanobubbles that is stable against dissolution. Diffusive equilibrium requires that the concentration of gas at the bubble surface equals the concentration c_1 of gas dissolved in the liquid. Henry's law then implies that $p_{eq} = p_0 c_1 = c_0$, where p_{eq} (p_0) is the equilibrium pressure in the bubble (liquid), and c_0 is the dissolved (saturated) gas concentration. The difficulty with nanobubble stability is that according to the ordinary Laplace law, $p_{eq} - p_0 = 2 \gamma / R_0$, where γ is the liquid-gas surface tension and R_0 the radius of curvature of the bubble. Thus force equilibrium is inconsistent with diffusive stability [34]! If stable nanobubbles exist, the Laplace law must be violated on these length scales. The origin of this departure, although not clear, is probably due to significant contributions from intermolecular effects (bubble size \sim Hamaker length) and electrical effects (bubble size \sim Debye-Huckel screening length).

We therefore use the following generic model for nanobubble stability: we modify the Laplace law by

$$p_{eq} - p_0 = \frac{2 \gamma}{R_0} f(R_0) \quad (7)$$

Here f is a phenomenological function taking into account the (yet unknown) forces that stabilize the bubble (θ is the liquid-solid contact angle), with $R_0 f(R_0) \rightarrow 0$ as $R_0 \rightarrow 1$, so that the Laplace law is recovered in the macroscopic limit; as will be seen in section V, the fit to the data of Zhu & Granick [8] depends in fact very weakly on the exact profile of $f(R_0)$.

Note that a microscopic model might lead to a more general f , depending explicitly for example on the height of the bubbles, which shape as a result will not be spherical. Given the current knowledge of nanobubbles, we will

consider in this paper a simplified description and we will assume for simplicity that f is only a function of the bubble radius, which shape is therefore assumed to be spherical. If $V = V(R)^3$ is the volume of a single bubble, then the average thickness of the gas layer is $h(t) = nV(R(t))^3$. For spherical bubbles with (θ) as the interior angle (see Figure 1), we have $V(\theta) = (1 + \cos \theta)^2 (2 - \cos \theta) = 3$.

IV. INFLUENCE OF NANOBUBBLES ON FORCE MEASUREMENTS

We study in this section the perturbations about the equilibrium described by (7) and their consequences on force measurements.

A. Gas compression

Let us consider the response of the bubbles to an external force F between the plates; this changes the liquid pressure from p_0 to p , and the pressure in the bubbles from p_{eq} to p_b . Here, S is the typical value of the sphere surface on which the viscous force acts $S = \pi L^2$ and L the radial geometrical length scale $L = (aD)^{1/2}$. At the small frequencies typical of squeeze flow experiments ($1-10^2$ Hz), the gas is isothermal, so the pressure in the bubble changes via the ideal gas law $p_b R^3 = p_{eq} R_0^3$, where R_0 is also allowed to change in time to account for gas diffusion into (and out of) the equilibrium bubble. For small oscillations, the radius change is therefore

$$\frac{R - R_0}{R_0} = \frac{p_{eq} - p_b}{3p_{eq}} \quad (8)$$

In order for this radius change to be related to the applied force F we need to relate the change in bubble pressure to that in the liquid. Combining a perturbation of (7) around equilibrium with Henry's law and the ideal gas law leads to the relation between the dimensionless increases in pressure in both the bubble and the bulk

$$\frac{p_b - p_{eq}}{p_{eq}} = \frac{p - p_0}{p_0} \quad (9)$$

where

$$\beta = \frac{c_1}{c_0} \frac{R_0 f'(R_0)}{3p_0} \frac{2}{3R_0 p_0} \quad (10)$$

It is easily verified that in the case of nanobubbles for which $\beta = R_0 p_0 > 1$, any $f(R) = R^\alpha$ with $\alpha > 1$ leads to $\beta > 0$ so that a pressure change in the bubble is positively correlated with that in the bulk.

The viscous force on the sphere can now be directly related to the change in radius. Combining $F = (p - p_b)S$ with the ideal gas law and (9), we obtain $R = R_0 (1 + \beta \frac{F}{p_0 S})$; hence using $h = nV(R)^3$, the rate of change of the mean bubble height h is given by

$$\frac{dh}{dt} = \frac{dh_0}{dt} + \frac{3 h_0}{p_0 S} \frac{dF}{dt}; \quad (11)$$

where $h_0 = h_0(t) = nV R_0^3$. We thus have that the rate of change of the mean bubble height is the sum of the rate of change of the mean equilibrium bubble height h_0 , governed by gas diffusion, plus the second contribution due to the gas compressibility.

B. Gas diffusion

We now consider the rate of gas diffusion from the bubble. In our model for the oscillatory squeeze flow experiments [2, 6, 8], bubbles lose mass by both vertical diffusion across the liquid layer and radial diffusion along the apparatus; because of the scale separation $D \gg a$, these two processes require separate treatment.

Let us first consider the case of vertical diffusion. Since for most common gases, $D \approx 10^{-9} \text{ m}^2/\text{s}$, the vertical oscillatory Peclet number, $Pe_v = D/\delta = \dots$, is always smaller than unity in the reported experiments: on the experimental time scale δ^{-1} , the bubbles are approximately in instantaneous vertical diffusive equilibrium. The dissolved gas concentration above the bubble is therefore uniform throughout the liquid gap and is given, in the case of small amplitude oscillations, by Henry's law $c = p_b c_1 = p_{eq}$. The number of gas molecules N per unit area necessary to fill the liquid gap at this concentration is equal to the gap thickness $(D - 2h_0)$ times the change in concentration $c_1 (p_b = p_{eq} - 1)$. Using (9) we get that N is proportional to the viscous force

$$N = \frac{c_1 (D - 2h_0)}{p_0 S} F; \quad (12)$$

Since by definition, the instantaneous number of gas molecules per unit area is equal to $c_1 - c_0 = c_0$, the rate of change of h_0 is given by

$$\frac{dh_0}{dt} = \frac{dh_{0r}}{dt} - \frac{c_0}{c_1 - c_0} \frac{dN}{dt} = \frac{dh_{0r}}{dt} - \frac{c_0 (D - 2h_0)}{p_0 S} \frac{dF}{dt} \quad (13)$$

where dh_{0r}/dt is the rate of change in the mean bubble height governed by gas diffusion in the (slowly varying) radial direction of the apparatus; let us now evaluate this contribution.

In contrast to the vertical case, the radial oscillatory Peclet number, $Pe_r = L^2/\delta = \dots$, is of order unity or larger, so that radial diffusion has to be accounted for explicitly. Assuming the dissolved gas is in vertical diffusive equilibrium, the time rate of change of the mass of a gas bubble dm/dt is given by a flux integral on the bubble surface S_b

$$\frac{dm}{dt} = \int_{S_b} n_r c \, dS = 4\pi R^2 \left(\frac{\partial c}{\partial r} \right); \quad (14)$$

where assuming a spherical bubble implies $I(\theta) = (2 \cos^2 \theta + \sin^2 \theta) = 2$. In general, the radial concentration of dissolved gas $c(r;t)$ verifies an advection-diffusion equation with shear dependent diffusivity [35]. However, for the small amplitude oscillation in [8], both advection and Taylor dispersion are negligible, and $c(r;t)$ satisfies a pure diffusion equation. We locally approximate radial concentration gradient by a simple linear law $\partial c/\partial r = (c_1 - c_0)/L_r$ where $L_r = (\delta)^{1/2} = L = P \delta^{1/2}$ is the typical (shear dependent) radial gradient length scale. When evaluating the bubble mass at the equilibrium pressure p_{eq} , $m = V (p_{eq}) c_1 = c_0 = h_0 c_1 = c_0 n$, equation (14) together with Henry's law leads to a linear relation between the rate of change of h_{0r} and the viscous force

$$\frac{dh_{0r}}{dt} = \frac{R_0^2 I(\theta) n c_0}{p_0 S L_r} F \quad (15)$$

C. Final formula for the force ratio

With (11), (13) and (15), we obtain that the mean bubble height h satisfies the differential equation

$$\frac{dh}{dt} = k_1 F - k_2 \frac{dF}{dt}; \quad (16)$$

where $(k_1; k_2)$ are given by

$$k_1 = \frac{n R_0^2 I(\theta) c_0}{p_0 S L_r}; k_2 = \frac{3 h_0 c_0 + c_0 (D - 2h_0)}{p_0 S} \quad (17)$$

Together with (5), (16) leads to a linear ordinary differential equation for the force F given by

$$F(t) = f \frac{6 \alpha^2}{D} V_s + k_1 F + k_2 \frac{dF}{dt} \quad (18)$$

With a sinusoidal sphere velocity $V_s = \frac{d}{dt} (d \sin \omega t)$, and if we denote $\omega = 2\pi f = D$ for clarity, the solution to (18) with no force at $t=0$ is given by

$$F(t) = \frac{1}{2} \frac{d(1+k_1)}{(1+k_1)^2 + (\omega k_2)^2} \cos \omega t - e^{-\frac{1+k_1}{k_2} t} + \frac{\omega k_2}{1+k_1} \sin \omega t \quad (19)$$

After an exponentially decaying transient occurring on a time scale $\tau = (1+k_1)/k_2$, the ratio of the force out-of-phase with the sphere displacement to that expected (3) with no-slip and no bubbles is given by

$$\bar{f} = \frac{f(1+k_1)}{(1+k_1)^2 + (\omega k_2)^2}; \quad (20)$$

which is also equation (6). The new force ratio we obtain $\bar{f} < 1$ is also smaller than that given by the non-zero slip length $\bar{f} < f$, so that the "leaking mattress" mechanism we propose leads to an additional apparent slip effect, of dynamic origin. The effect is shear-dependent through the frequency dependence in (20): higher frequency and therefore higher shear rates lead to a larger apparent slip, in agreement with [2, 7, 8]. However, the model assumes small amplitude oscillations which consequently does not appear in the final formula for f .

We finally note from (19) that the force on the sphere also contains a non-zero component in-phase with the displacement of the sphere, and therefore out-of-phase with its velocity. If we denote by g the ratio of this in-phase response to the expected no-slip no-bubbles out-of-phase response, we obtain

$$g = \frac{f \omega k_2}{(1+k_1)^2 + (\omega k_2)^2} = \frac{\omega k_2}{1+k_1} \bar{f} \quad (21)$$

Equation (21) is a prediction of the effective elasticity provided by the nanobubbles to the surface and is experimentally testable. The values of the in-phase responses of the forces were unfortunately not reported by Zhu & Granick [8].

V. COMPARISON WITH EXPERIMENTS AND DISCUSSION

We present in this section a quantitative comparison of our model with the experimental results of Zhu & Granick in the case of deionized water, namely the four sets of data presented in Figure 2 of ref [8]. The macroscopic water/solid contact angle in this case was 110° and we assumed that the liquid was saturated with O_2 at 25 C and 1 atm, for which $\rho_0 = 1.28 \text{ kg/m}^3$, $c_0 = 8.3 \cdot 10^{-3} \text{ kg/m}^3$ and $\gamma = 2 \cdot 10^{-9} \text{ m}^2/\text{s}$.

The "leaking mattress" model we have presented in the previous sections has four free parameters which we will explore in order to provide an adequate fit to the experimental data: (a) the stabilizing mechanism for the nanobubbles, described by the derivative $f^0(R_0)$ (in equation 10); we chose to describe it by the dimensionless parameter defined by

$$= R_0 \frac{f^0(R_0)}{f(R_0)} \quad (22)$$

so that > 1 and equation (10) becomes

$$1 = \frac{c_1}{c_0} \left(1 - \frac{1}{3} + \frac{1}{3} + \frac{2}{3R_0 p_0} \right); \quad (23)$$

(b) the size of the spherical bubbles, described by their radius of curvature R_0 , (c) the area fraction of the bubbles on the surface, $0 < \phi < 1$, and (d) the microscopic contact angle at the bubble level; significantly differs from the macroscopic contact angle because of both intermolecular forces and electrical effects at the nanometer scale.

To reduce the set of free parameters available we will enforce the following geometrical condition: we will require that the two layers of bubbles fit in the gap between the sphere and the plane for all separation distance in each experiment. This can be written as

$$2h_0 = 2R_0(1 + \cos \theta) \quad \text{in } (D): \quad (24)$$

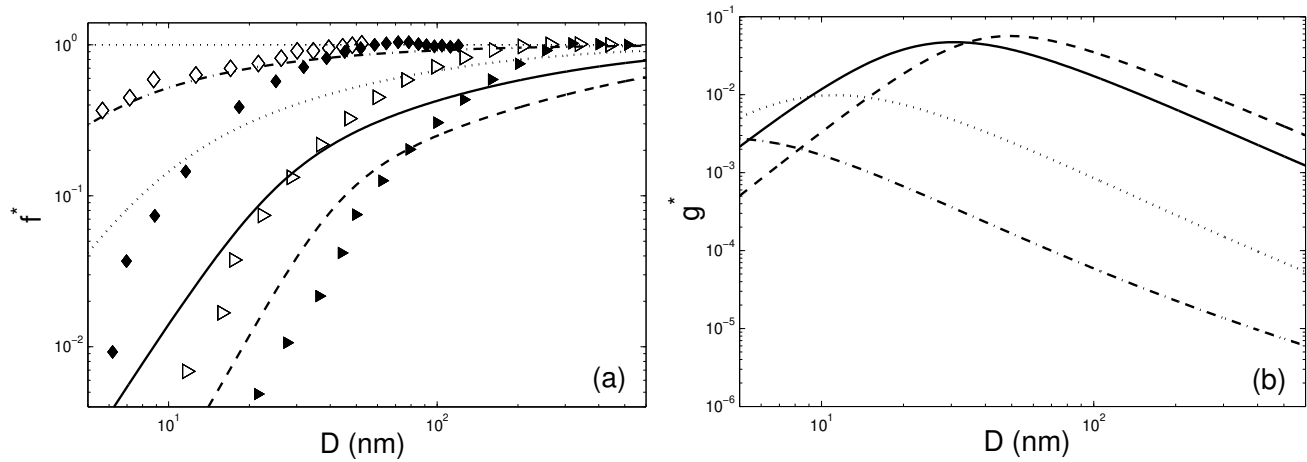


FIG. 2: (a): Example of comparison between the experimental data of Zhu & Granick (2001) and the dynamic model with $\beta = 3=2$. (\diamond): data for $d = 0.5$ nm, $\omega = 1$ Hz; dashed-dotted line: model for $R_0 = 8$ nm, $\beta = 160$ and $\gamma = 95\%$; (\triangle): data for $d = 6$ nm, $\omega = 1$ Hz; dotted line: model for $R_0 = 50$ nm, $\beta = 160$ and $\gamma = 95\%$; (\circ): data for $d = 1.6$ nm, $\omega = 10$ Hz; solid line: model for $R_0 = 100$ nm, $\beta = 160$ and $\gamma = 99\%$; (\square): data for $d = 6$ nm, $\omega = 10$ Hz; dashed line: model for $R_0 = 400$ nm, $\beta = 167$ and $\gamma = 99\%$. (b): Prediction for the effective elasticity provided by the nanobubbles to the solid surfaces; the four curves correspond to the same parameters as in (a).

By doing so, we restrict ourselves to the case of non-bridging bubbles.

Further, a value for the slip length that appears in equation (4) has to be chosen. We chose not to use the estimate given in equation (2) because a set of gas bubbles on a surface present a higher collective resistance to fluid motion than a gas layer. First the bubbles have curved interfaces along which flow has to occur, which increases the viscous dissipation in their vicinity and therefore reduces the effective slip length for flow over the surface [3]; the same argument applies for rough surfaces [4]. This effect is however attenuated when the bubbles are very flat, which seems to be the case in experimental observations of nanobubbles, as shown by the AFM measurements in [22, 23]. Second, flow over an array of surface-attached bubbles, be they very flat, satisfies mixed boundary conditions: no-slip on the portion of the surface that is not covered by bubbles and (almost) perfect slip on the bubble surface. Such mixed configuration was studied in detail in [18, 36] where it was shown that, in the limit where the surface on which the bubbles sit is almost flat, a mix of slip and no-slip boundary conditions lead to logarithmically dependent slip lengths,

$$\frac{H}{\lambda} \ln \sec \frac{\alpha}{2} \quad (25)$$

where H is the typical distance between the centers of two bubbles $H = 2R_0 \sin \alpha = \lambda/2$.

The experimental data in [8] are found to be relatively well predicted by our simple model (6), as illustrated in Figure 2a. In all cases, the contribution to the decrease in f^* due to vertical diffusion is negligible; when $\omega = 10$ Hz, most (approximately 80%) of the decrease in f^* is due to compression; when $\omega = 1$ Hz, compression and radial diffusion are comparable. We also present in Figure 2b our prediction for the in-phase response of the force g^* , given by equation (21), for the same values of the parameters as in Figure 2a. Note that g^* does not vary monotonically with D .

The fits in Figure 2 were obtained for particular values of f^* ; R_0 ; β ; γ . We present in Figure 3 the range of values for each of the free parameters which lead the best fit (and within 10% of the best fit) to the four data sets from Zhu & Granick. The results are plotted in the form of R_0 as a function of β with γ and f^* fixed (Fig 3a); R_0 as a function of β with γ and f^* fixed (Fig 3b); R_0 as a function of β with γ and f^* fixed (Fig 3c). As a matter of comparison, we have

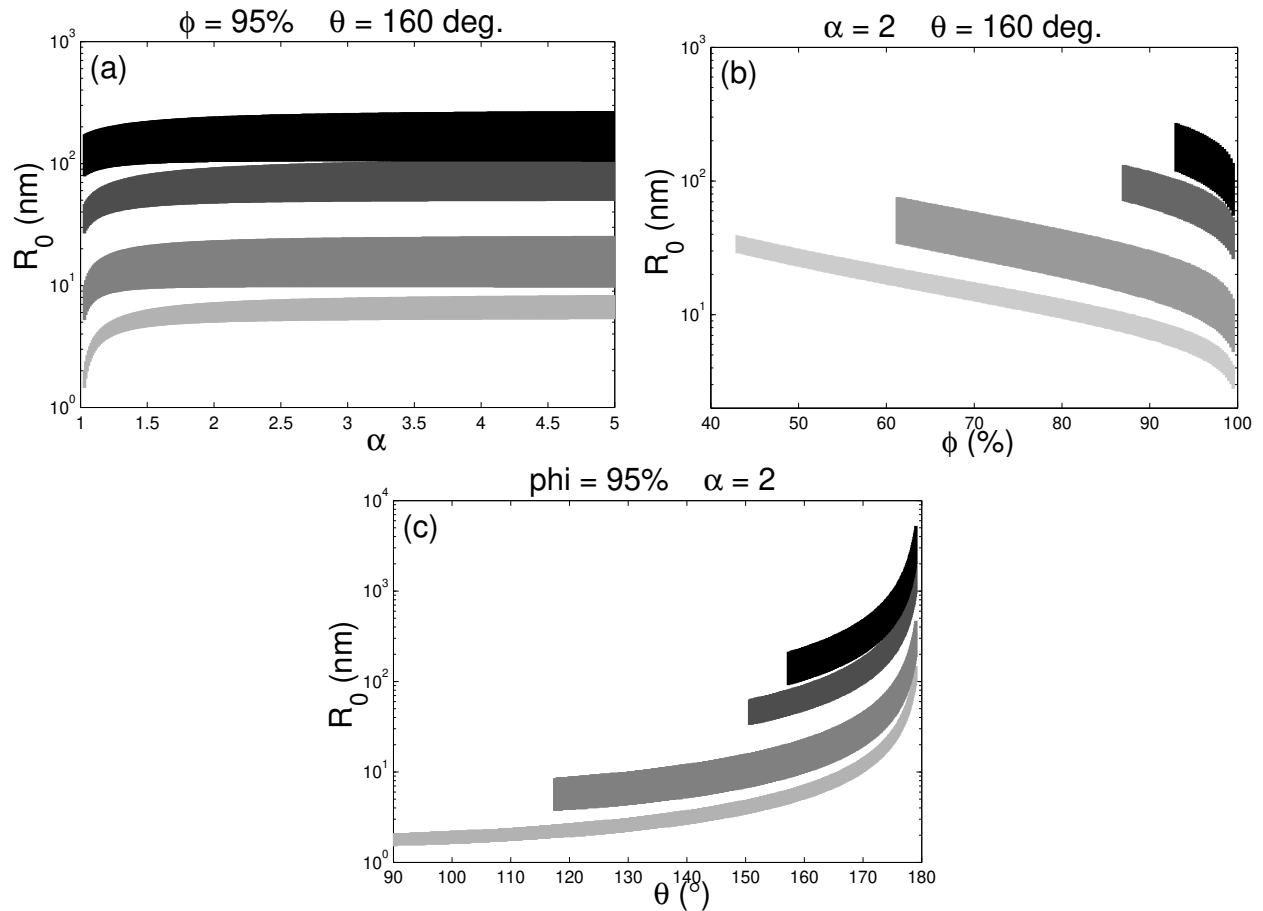


FIG. 3: Fit of the data of Zhu & Granick (2001) by the model: (a) radius of curvature of the nanobubbles (nm) as a function of the surface coverage (%) for a microscopic contact angle of 160 and $\alpha = 2$; (b): radius of curvature as a function of the microscopic contact angle ($^\circ$) for a surface coverage $\phi = 95\%$ and $\alpha = 2$; (c): radius of curvature as a function of the power of the stabilizing mechanism, for a microscopic contact angle of 160 and a surface coverage $\phi = 95\%$. The data corresponds to experiments for which $f = 1$ Hz and $d = 0.5$ nm (light grey); $f = 1$ Hz and $d = 6$ nm (grey); $f = 10$ Hz and $d = 1.6$ nm (dark grey); $f = 10$ Hz and $d = 6$ nm (black).

summarized in Table I the experimental results of [21, 22, 23, 24] on the typical size, distribution and morphology of nanobubbles observed by atomic force microscopy.

First, the results displayed on Fig 3a show that, for a given experiment, the bubble size is almost independent of the coefficient α , i.e. of the exact profile of the mechanism stabilizing the nanobubbles against dissolution. This result shows that our study is able to quantify the influence of these bubbles on force measurement even if we do not understand yet the mechanism responsible for their stability.

Further, Fig 3b and c show that if we require the same contact angle and surface coverage to fit all the data, then the surface coverage has to be sufficiently high ($\phi \approx 90\%$) and the bubbles need to be sufficiently flat ($\theta \approx 155^\circ$). This compares very favorably with the experimental evidence of nanobubbles in [21, 22, 23, 24] and summarized in Table I. In all cases, nanobubbles were found to be flat with large water/surface microscopic contact angle and in three out of four studies, the bubbles were found to cover almost entirely the solid surface. As a difference, the pictures in [21] show bubbles with lower surface coverage. We also note that our previous study of slip in pressure-driven flow experiments lead to a similar conclusion: in order for surface-attached bubbles to be responsible for the measured slip, surface coverage of almost 100% was necessary [18].

	Ishida et al. [21]	Tyrrell & Attard [22]	Tyrrell & Attard [23]	Steitz et al. [24]
Projected area (nm ²)	3.3 · 10 ⁶	4 · 6 · 10 ⁶	4 · 7 · 10 ⁶	2 · 11 · 10 ⁶
Height h ₀ (nm)	40	20 · 30	20 · 30	< 18
Radius of curvature R ₀ (nm)	1300	50	40 · 60	30 · 100
Surface coverage	20%	100%	100%	89%
Macroscopic contact angle	110	101	101	> 90
Microscopic contact angle	166	120	117 · 130	130 · 147

TABLE I: Summary of experimental data on nanobubbles as found in [21, 22, 23, 24] by atomic force microscopy: projected area of each bubble on the solid surfaces, height above the surfaces h_0 , radius of curvature R_0 , surface coverage, macroscopic and microscopic contact angle. The radius of curvature and microscopic contact angles were inferred from the other data assuming spherical cap nanobubbles.

Finally, Figure 3 shows that a large range of bubble sizes is consistent with the four sets of experimental data. However, for a given value of the surface coverage and the contact angle, the range of R_0 between the four experiments is less than 2 orders of magnitude; for example, the data in Figure 3b show a ratio of about 20 between the maximum typical radius (black data, $R_0 = 200$ nm) and minimum typical radius (light grey data, $R_0 = 10$ nm) necessary to predict the corresponding measurements. These results are quantitatively consistent with the experimental data for bubble sizes presented in Table I.

The fact that our model predicts different bubble sizes for different experiments could be a sign that even in similar experimental conditions large fluctuations in bubble sizes should be expected; as a matter of comparison, the data in [23] show large standard deviation (up to 70%) for the bubble area. Also the bubbles might not just be a surface property but could depend on the experimental procedure used to prepare the surfaces and their manipulation in and out of the liquid bath.

Alternatively, this result could hint at the possibility of bubbles with dynamically selected sizes. It has been reported experimentally in [37] that the jump-in distance between two hydrophobic surfaces in water, believed to be due to the presence of nanobubbles, depended on the history of the sample; performing the experiment several times lead to changes in the jump-in distances over time which was found to remain constant only after a few periods. A similar scenario could be envisioned in our case.

VI. CONCLUSION

We have explored in this paper the consequences of the presence of nanobubbles on the surfaces where squeeze flow experiments are performed. We have shown that, within the framework of a simple stabilizing model, the dynamics of nanobubbles always leads naturally to a shear-dependent decrease in the measured viscous force by a "leaking mattress" effect: as the solid sphere oscillates, periodic bubble compression and disunion reduces the amount of liquid necessary to be squeezed out of the gap and thereby the force on the moving sphere.

We emphasize that this mechanism is of dynamic origin, and is not a consequence of the microscopic slip at the bubble surfaces; in particular, we argue that this is why shear-dependent slip length have not been reported by investigations of slip in pressure-driven flow experiments, where no oscillatory pressure is present to trigger an effect similar to the one proposed here. Also, the mechanism we propose should also apply to squeeze flow experiments performed on super-hydrophobic surfaces such those reported in [38] with small air bubbles trapped on fractal surfaces.

We also note that the final formula for the force ratio \bar{f} shows that the apparent slip due to the "leaking mattress" effect increases with the fluid viscosity, in agreement with experiments [7, 10]; it also increases with the size of the sphere a , which might account for the large slip lengths reported in [8] (cm-size spheres) as opposed to other squeeze flow experiments (usually μ -size spheres). The measured overall apparent slip length is therefore not only a solid/liquid property but depends on the system size [18].

The calculations on the model have been performed with several simplifying assumptions and, in particular, additional contributions to the sets of coefficients ($k_1; k_2$) could come from bridging bubbles, large amplitude oscillations of the solid sphere, bubble interactions, deformation or displacement on the solid surface.

We have then presented a comparison between the predictions of our model when applied to the experiments of Zhu & Granick and available experimental data on nanobubbles in order to determine their characteristic features. Quantitative agreement was obtained concerning on the bubbles sizes, their distribution on the solid surfaces and their shape. Further, we have shown that the conclusions of our study are virtually independent of the stabilizing model chosen for the nanobubbles. Finally, a formula has been proposed for the effective elasticity provided by the bubbles to the solid surface.

To conclude, we present a simple prediction based on the results of our model. If a squeeze flow experiment was performed with two different surfaces, say a hydrophobic plane and a hydrophilic sphere, force ratio measurements displaying shear-dependant results should be able to test whether the ideas put forward in this paper are valid. Indeed, if the force decreases was really due, not to bubbles, but to a change in the hydrodynamic boundary condition for flow past the hydrophobic surface, the maximum force decrease one could expect to obtain is $1=4$ for the case of a perfectly slipping surface (see [33] for the calculation; this result can also be found by symmetry about the plane where slip occurs). If alternatively the measurements are due to a "leaking mattress" effect similar to the one we propose here, equation (5) should also apply (with different prefactors) and therefore so is equation (6); consequently, force ratio smaller than $1=4$ should be obtained in this case. This proposition for an experiment, together with the prediction for the in-phase response of the force (equation 21), would allow our model to be tested experimentally.

Acknowledgments We are grateful to Jacquie Ashmore, Todd Squires, Jose Gordillo, Steve Granick and Howard Stone for useful discussions. This research was supported by the Harvard MRSEC, and the NSF Division of Mathematical Sciences.

-
- [1] Goldstein S. Modern Developments in Fluid Dynamics, vol. II (1938) 676 (Clarendon Press).
- [2] Zhu, X. and Granick, S. Phys. Rev. Lett. 88 (2002) 106102.
- [3] Jansons, K M. Phys. Fluids 31 (1988) 15.
- [4] Richardson, S. J. Fluid Mech. 59 (1973) 707.
- [5] Pit, R., Hervet, H. and Leger, L. Phys. Rev. Lett. 85 (2000) 980.
- [6] Baudry, J., Charlaix, E., Tonck, A. and Mazuyer, D. Langmuir 17 (2001) 5232.
- [7] Craig, V S J., Neto, C. and Williams, D R M. Phys. Rev. Lett. 87 (2001) 054504.
- [8] Zhu, X. and Granick, S. Phys. Rev. Lett. 87 (2001) 096105.
- [9] Bonaccorso, E., Kappl, M. and Butt, H.-S. Phys. Rev. Lett. 88 (2002) 076103.
- [10] Cheng, J.-T. and Giordano, N. Phys. Rev. E 65 (2002) 031206.
- [11] Tretoway, D C. and Meinhart, C D. Phys. Fluids 14 (2002) L9.
- [12] Cottin-Bizonne, C., Jurine, S., Baudry, J., Crassous, J., Restagno, F. and Charlaix, E. Eur. Phys. J. E 9 (2002) 47.
- [13] Thompson, P A. and Troian, S M. Nature 389 (1997) 360.
- [14] Barrat, J.-L. and Bocquet, L. Phys. Rev. Lett. 82 (1999) 4671.
- [15] Brenner, H. and Ganesan, V. Phys. Rev. E 61 (2000) 6879.
- [16] Cieplak, M., Koplik, J. and Banavar, J R. Phys. Rev. Lett. 86 (2001) 803-806.

- [17] Denniston, C. and Robbins, M. O. *Phys. Rev. Lett.* 87 (2001) 178302.
- [18] Lauga, E. and Stone, H. A. *J. Fluid Mech.* (2003) 489–55.
- [19] de Gennes P. G. *Langmuir* 18 (2002) 3413.
- [20] Navier, C. L. M. H. *Mémoires de l'Académie Royale des Sciences de l'Institut de France VI* (1823) 389.
- [21] Ishida, N., Inoue, T., Miyahara, M. and Higashitani, K. *Langmuir* 16 (2000) 6377–6380.
- [22] Tyrrell, J. W. G. and Attard, P. *Phys. Rev. Lett.* 87 (2001) 176104.
- [23] Tyrrell, J. W. G. and Attard, P. *Langmuir* 18 (2002) 160.
- [24] Steitz, R., Gutberlet T., Hauss, T., Kłosgen, B., Krashev, R., Schimmel, S., Simonsen, A. C. and Findenegg, G. H. *Langmuir* 19 (2003) 2409.
- [25] Israelachvili J. *Intermolecular and Surface Forces* (1992) (Academic Press).
- [26] Carambassis, A., Jonker, L. C., Attard, P. and Rutland, M. W. *Phys. Rev. Lett.* 80 (1998) 5357.
- [27] Mahnke, J., Steames, J., Hayes, R. A., Fomasiero, D. and Ralston, J. (1999) *Phys. Chem. Chem. Phys.* 1, 2793–2798.
- [28] Attard, P. *Langmuir* 16 (2000) 4455–4466.
- [29] Yakubov, G. E., Butt, H.-S. and Vinogradova, O. I. *J. Phys. Chem. B* 104 (2000) 3407.
- [30] Schnell, E. J. *Appl. Phys.* 27 (1956) 1149.
- [31] Churaev, N. V., Sobolev, V. D. and Somov, A. N. *J. Colloid. Int. Sci.* 97 (1984) 574.
- [32] Watanabe, K., Udagawa, Y., and Udagawa, H. *J. Fluid Mech.* 381 (1999) 225.
- [33] Vinogradova, O. I. *Langmuir* 11 (1995) 2213.
- [34] Ljunggren S. and Eriksson J.C. *Colloids Surf. A* 129–130 (1997) 151.
- [35] Taylor, G. I. *Proc. Roy. Soc. A* 219 (1953) 186.
- [36] Philip, J.R. *J. Appl. Math. and Phys. (Zeitschrift für Angewandte Mathematik und Physik)* 23 (1972) 353.
- [37] Yakubov, G. E., Butt, H.-J. and Vinogradova, O. I. *J. Phys. Chem. B* 104 (2000) 3407.
- [38] Onda, T., Shibuichi, S., Satoh, N. and Tsuji, K. 1996 *Langmuir* 12, 2125.